Thesis for the degree
Master of Science

Submitted to the Scientific Council of the
Weizmann Institute of Science
Rehovot, Israel

עבודת גמר (תזה) לתואר
מוסמך למדעים

מוגשת למועצה המדעית של
מכון ויצמן למדע
רחובות, ישראל

By
Lior Neeman

מאת
ליאור נאמן

התקן התאבכות קוונטי מוליך-על על גבי חוד עם ליבה מגנטית לחקר מערבולות מגנטיות

SQUID on tip with a magnetic core for magnetic imaging of single vortices

Advisor:
Prof. Eli Zeldov

מנחה:
פרופ. אלי זלדוב

January 2011

שבט תשע"א

Abstract

In this work we describe the efforts made in order to upgrade a novel tip for a scanning SQUID (Superconducting QUantum Interference Device) microscope (SSM)[1], to contain a magnetic core for magnetic flux enhancement. A tip with a SQUID has been fabricated by pulling a quartz tube up to a submicron diameter (typically 250 nm outer diameter). Then, a SQUID is produced by thermal evaporation of Pb on the quartz tip from three directions. The aforementioned quartz tube must contain a quartz filament embedded from within to allow for capillary action of liquids, that will be employed to fill it with a solution of magnetite (Fe_3O_4) nanoparticles, 6 nm in size, in paraffin oil and toluene. Letting the solution to dry in air, all the liquids evaporate and the magnetite nanoparticles remain at the tip's sharp end and should act as a magnetic flux concentrator for the SQUID. This novel device should operate at liquid He temperature of 4.2 K and increase the magnetic sensitivity of the existing SQUID-on-a-tip which has already been achieved with aluminum and lead SQUIDs.

Other ways of producing a magnetic core in the tip such as pulling magnetic metallic wires together with the quartz tube, or plating the interior of the tubes prior to and after pulling the tips, were tested and found unsuccessful. The method of the magnetite nanoparticles filling, however, proved to be feasible and reproducible. The Pb SQUID-on-a-tip fabrication is reproducible as well, although not at a satisfactory success rate.

A measurement of a complete device that contains magnetite nanoparticles embedded in a core of a Pb SQUID tip had yet to be accomplished.

Contents

Appendices

1. Introduction

Over the past decades, there has been a growing interest in developing magnetic imaging techniques with the highest possible spatial resolution and highest field sensitivity. Popular imaging techniques capable of resolving single vortices in superconductors (see section 1.1.1 for more information) include the methods of Bitter decoration[2], scanning tunneling microscopy (STM)[3] scanning Hall probe microscopy (SHM)[4], magnetic force microscopy (MFM)[5], Lorentz microscopy[6], scanning SQUID microscopy (SSM)[7] and others. The technique used by us is the scanning SQUID microscopy, in which a dc SQUID is scanned across the sample surface to measure its local fields.

In the field of SSMs, there exist many SQUID designs which are planar due to their lithographic fabrication process. Such SQUIDs have a major drawback in their sample-SQUID relatively large distance. Some have examined a solution to this problem by using a magnetic needle to enhance the magnetic signals and transport it from the sample surface to the SQUID's loop[8, 9, 10, 11, 12, 13]. Our proposed idea will enjoy both the scanning abilities of our SQUID-on-a-tip, which is a SQUID that is placed at the apex of a very sharp quartz tip and allow for minimal tip-sample distance, and the magnetic amplification of a flux focusing core as well.

In this chapter we will present a short introduction to superconductivity, SQUIDs and flux focusing with a specific section describing nanoparticles basics. The experimental setup and methods will be presented here as well.

1.1 Theory

1.1.1 Superconductivity

Superconductivity is a state of matter that displays zero resistivity when below a critical temperature and also completely expels weak magnetic fields from its bulk (known as the Meissner effect). The superconductors (SC) are categorized into two types (see section 1.1.1.1 for more details), where type I SCs obeying the above two phenomena. Type II SCs, however, can show resistance and allow for field penetration even when the material is still considered superconducting.

Superconductivity was first discovered by chance, when Onnes[14] cooled down mercury with liquid He in 1911 and witnessed a sudden drop in resistivity to a unmeasurably low value. Subsequently, many other SC have been discovered, but the theories offered to describe them were debateable. The first widely accepted theoretical understanding of superconductivity was achieved in 1957 by Bardeen, Cooper and Schrieffer, and is called the BCS theory[15]. BCS theory explained the superconducting current as a superfluid of bosonic Cooper pairs, pairs of fermionic electrons interacting through the exchange of lattice phonons with an energy gap for excitations. This theory explained the behavior of classic SCs. However, in 1986 another type of SCs was discovered by Müller and Bednorz[16] - high temperature SCs. This new type obeyed the general phenomenology of the classic SCs, but its microscopic mechanism remains an open question. Long before the microscopic theory, in 1950, a phenomenological approach to superconductivity had been proposed by Ginzburg and Landau[17]. It is based on the idea that the normal superconducting transition is, in the absence of a magnetic field, a thermodynamical second-order transition. Thus, one can apply to it the general theory of second order transitions and define an order parameter ψ which is zero in the disordered state (the normal material) and finite in the ordered state (the superconducting material). The two approaches, microscopic and phenomenological, remained completely separate until Gor'kov[18], in 1959, showed that in some limiting cases, the order parameter of the phenomenological equations and the pair potential of the microscopic theory are proportional.

1.1.1.1 Type I and type II Superconductors

There are two main characteristic length scales for SCs. The coherence length ξ, which characterizes the distance over which the order parameter can vary and the London penetration depth λ, which characterizes the distance over which the magnetic field can vary. Their dimensionless ratio $\kappa = \lambda/\xi$ was shown to be of great importance by Abrikosov in 1957[19]. $\kappa = \sqrt{1/2}$ is the critical value, separating between two types of SCs. Type-I SCs ($\kappa < \sqrt{1/2}$) fully expel the magnetic field from their bulk at T¡T$_c$. However, when a critical magnetic field (H$_c$) or critical current density (j$_c$) is applied, type-I SCs allow for the field to penetrate the bulk and destroy superconductivity completely. Type-II SCs, however, have two critical fields. Upon applying a magnetic field as high as the first critical field H$_{c1}$, it is energetically favorable for the magnetic flux to enter the superconductor in domains of characteristic length ξ in which the material is normal, while its surrounding material remains superconducting. Abrikosov showed that the flux penetrates in a regular array of flux tubes , that are called *vortices*, since there are circulating supercurrents around each tube, which act to quantize the flux in each tube to a flux quantum of $\phi_0 = hc/2e$ (fluxon). When the field is raised, the vortices arrange in a triangular lattice, which grows denser with the increasing field, up to the second critical field H$_{c2}$, where the superconductivity is entirely destroyed.

1.1.2 SQUID (Superconducting Quantum Interference Device)

A SQUID is a device that consists of a superconducting loop with two Josephson Junctions (JJ) connected in parallel. In order to explain how a SQUID works, we shall first introduce the principles of the Josephson Junctions.

1.1.2.1 Josephson Junction

In 1962 B. D. Josephson[20] predicted that a current should flow between two superconducting electrodes separated by a thin insulating barrier even with no applied voltage between them. This current is due to a different Ginzburg-Landau phase of the super-

conducting electrodes and is

$$I_s = I_c \sin(\Delta\phi). \tag{1.1}$$

Here I_c is the critical current which is the maximal current the junction can support and $\Delta\phi$ is the phase difference. Furthermore, he predicted that for a given applied voltage the phase difference will evolve in time creating an oscillating current with the frequency of $d(\Delta\phi)/d(t) = 2eV/\hbar$. These effects are called the DC and AC Josephson effects respectively.

Josephson junctions, in general, have hysteretic I-V characteristics. Without going into details, this hysteresis can be diminished by adding a suitable shunt resistor in parallel with the junction. Such a shunted junction is called an overdamped junction and its I-V curve can be seen in figure 1.1.

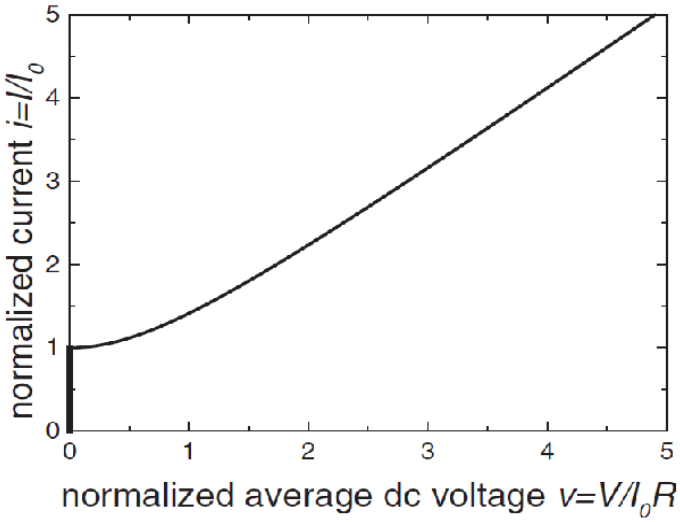

Fig. 1.1: *Characteristic I-V curve of an overdamped Josephson junction.*

Below the critical current the voltage is zero and above it the voltage-current function is described by equation (1.2), which smoothly interpolates between $V = 0$ for $I = I_{c0}$ to Ohm's law for $I \gg I_{c0}$. I_{c0} stands for the critical current at T=0 K.

$$V = R\sqrt{I^2 - I_{c0}^2}. \tag{1.2}$$

The effect was later generalized to any two strongly superconducting electrodes that

are separated by a "weak link" which is not necessarily an isolator, but could also be a normal conductor or a constriction (an area with a smaller cross section). These are referred to as S-I-S, S-N-S and S-c-S respectively. The JJs that are discussed hereafter are of the constriction kind.

1.1.2.2 The SQUID

The DC SQUID consists of two Josephson junctions connected in parallel on a superconducting loop. The maximum supercurrent that can flow across the ring is given by the sum of the critical currents of the two junctions and is modulated by the magnetic flux enclosed inside the SQUID ring with a period of one flux quantum. The reason for the modulation is the interference between the two superconducting wave functions in the two SQUID arms due to the closed loop and the demand for a single-valued wave function. In a case where both junctions have similar I_c, one can show that the maximal supercurrent I_m through the SQUID, which defines the SQUID's critical current is[21]

$$I_m = 2I_c|\cos(\pi\Phi/\Phi_0)|, \tag{1.3}$$

where Φ is the flux enclosed by the ring. When plugged into equation (1.2), assuming that the two arms have a similar resistance R, we get the oscillating dependance of the SQUID in the magnetic flux (for $I > I_m$).

$$V = \frac{R}{2}\sqrt{I^2 - (2I_c\cos(\pi\Phi/\Phi_0))^2} \tag{1.4}$$

This makes the SQUID a flux-to-voltage transformer, in which it is possible to detect changes in the applied magnetic flux corresponding to a tiny fraction of one flux quantum - typically $10^{-6}\Phi_0$. Its sensitivity is defined by the transfer coefficient $V_\phi = |(\partial V/\partial\phi)_I|$ evaluated at the maximal slope.

To operate a SQUID for measurements, a current at least as high as the critical current of the SQUID has to be applied, then it operates in the wanted resistive mode and there is a measurable voltage drop between the electrodes.

1.1.3 Flux Focusing

A magnetic guide is a piece of magnetic material with high permeability used to confine and guide magnetic fields. It is usually made of a ferromagnetic metal such as Iron, Cobalt or Nickel and their alloys, or ferrimagnetic compounds such as ferrites. In vacuum the magnetic field B equals the applied field H, but in a high permeability (high μ) material the magnetic field is many times larger than the applied field according to

$$H = \frac{B}{\mu}. \tag{1.5}$$

The high permeability, relative to the surrounding air or vacuum, causes the magnetic field lines to be concentrated in the core material.

This is a very appealing concept to be used in an SSM, in the form of a permeable material in the SQUID's loop, since it may increase the magnetic signal drastically. However, high permeability is not sufficient when coming to choose the material of the core for an SSM. Another, even more important, characteristic is low coercivity, that is to have the smallest magnetic hysteresis, so that the magnetization-field M(H) dependance will be an injective function (one-to-one) as much as possible. Table 1.1 presents the magnetic properties of some materials that can be employed.

Tab. 1.1: *Magnetic Properties of High-Permeability Metals and Alloys*

Material	Composition	Initial Permeability	Maximal Permeability	Coercive Force $[10^{-3}Oe]$	Saturation Polarization $[emu/cm^3]$
Iron,Fe	Commercial 99%	200	6000	880	1719
Iron,Fe	Pure 99.9%	25000	350000	10	1719
78 Permalloy	78Ni-22Fe	4000	100000	50	836
Supermalloy	79Ni-16Fe-5Mo	100000	1000000	1.9	629
Mu-metal	77Ni-16Fe-5Cu-2Cr	20000	100000	50	597
Magnetite	Fe_3O_4				477

All the data was taken from [22]. Some definitions: **Initial permeability** describes the permeability of a material at low values of B. **Maximal permeability** describes the maximal slope in the B-H diagram. **Coercive force** is the magnetizing field needed to reduce residual magnetism in a material to zero. **Saturation polarization**,in CGS units, is simply the magnetization at the saturation point .

Magnetic microscopy that employs this concept already exists. Many use a high permeability metal pointed tip as a magnetic flux guide (MFG) from the sample to the SQUID's loop[8, 9, 10, 11, 12, 13]. This method of flux guiding has its benefits such as improving the spatial resolution for large diameter SQUIDs while keeping its superior magnetic resolution, it also allows for several millimeters of separation between the sample, which can be at room temperature, to the SQUID, that need to be cooled (the separation is possible in the case of High-T_c superconductors that does not demand complicated cooling mechanism). Some even employ this metal tip as an STM sensor of the surface[12]. On the other hand such materials are not perfect MFGs in the sense that they exhibit flux losses along the tip's length (losses can be varied with the tip's geometry[11, 10]). When trying to measure extremely small magnetic fields those losses might become unacceptable. Magnetic materials can be used not only as flux guides, but as flux amplifiers if put in the middle of a SQUID loop, as was done by Golubović[23], who had grown a single domain Permalloy dot on the center of a SQUID loop for amplification. However, a magnetic material as a core for SQUIDs distorts the magnetic signal due to the magnetic hysteresis, saturated magnetization and the Barkhausen effect, which describes the sudden changes in magnetic domains in a multi-domain magnetic materials when it is being magnetized.

SQUID on a tip with flux core. A good integration of tip-sample proximity and a flux guide can be achieved by combining the novel scanning SQUID on a tip[1] with a magnetic core in the SQUID's loop. This way a superior magnetic sensitivity can be reached without enlarging the SQUID or putting it further away from the sample. This work follows the efforts made in order to accomplish this goal.

Few methods have been tested to insert magnetic material into the quartz tip: metal wires pulled together with the glass tubes, metal plating of the tube's interior and the use of magnetic nanoparticles in a suspension solution that fills the tip apex by capillary forces.

1.1.3.1 Magnetic Nanoparticles

As a particle size decreases below some critical value, the formation of domain walls becomes energetically unfavorable and the ferromagnetic particle can support only a single magnetic domain. This was long predicted in 1930 by Frenkel and Dorfman[24]. This critical size depends on the material and is usually on the order of tens to hundreds of nanometers. Magnetism in single domain particles is very different from multi-domain particles. In a multi domain structure, magnetization reversal occurs through the motion of domain walls, while in a single domain particles, the change in the direction of magnetization can occur only by coherent rotation of spins.

In many cases, the magnetic susceptibility of a material depends on the direction in which it is measured. Such a situation is called magnetic anisotropy and arises from the external shape of the particles, the imposed stresses and the crystalline structure itself. When magnetic anisotropy exists, the total magnetization of the system will prefer to lie along a special direction, called the easy axis (EA) of magnetization. For a fine single-domain particle, the energy associated with this alignment is called the anisotropy energy and can be written in the simplest approximation as

$$E_a = KV \sin^2 \theta, \tag{1.6}$$

where K is the anisotropy constant, V the particle volume, and θ the angle between the magnetic moment and the EA.

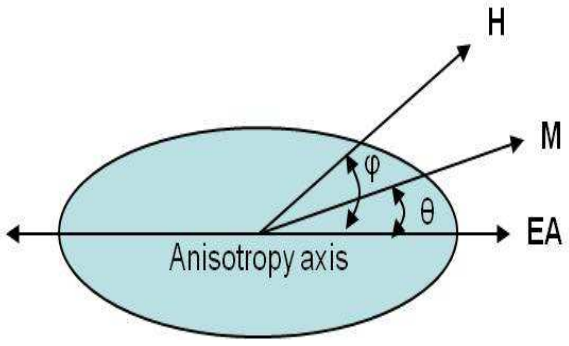

Fig. 1.2: *An illustration of a particle with only one asymmetry axis (easy axis EA), and an applied magnetic field H. The magnetization M finds its energetic minimum between the two.*

When an external magnetic field **H** interacts with the single-domain particle, an additional potential energy $E_f = -\mathbf{M_s} \cdot \mathbf{H}$ is added so that the energy to be minimized w.r.t θ is

$$E_{tot} = KVsin^2\theta - M_sH\cos(\theta - \varphi), \tag{1.7}$$

where φ is the angle between the applied magnetic field H and the EA, and M_s is the saturation magnetization (see figure 1.2).

This leads us to the understanding that if such a particle is fixed in space and has no thermal energy associated to it, it will have a different hysteresis curve at different applied magnetic field directions. For example, take a particle that is magnetized in one of the EA directions. If H is perpendicular to the EA we expect a minimal hysteresis because of the smooth transition between magnetic orientations. But, if H is antiparallel to the original magnetization it will have a maximal hysteresis curve. A detailed illustration is shown in figure 1.3.

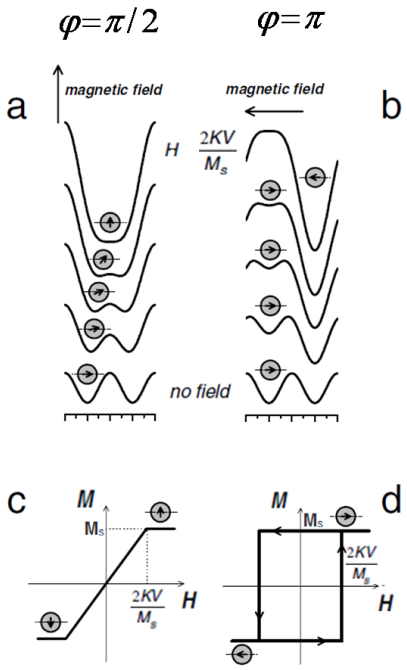

Fig. 1.3: *An illustration of a particle initially oriented at its easy axis direction and the potential it feels at 5 increasing values of applied magnetic field perpendicular (a) and anti parallel (b) to it. The arrows in the circles depicts the direction in which the particle is magnetized in each potential and the scale is the angle θ. (c) and (d) are the expected hysteresis curves of (a) and (b) respectively. Image is taken from [25]*

Another interesting phenomenon that happens due to the particle's small size is called *superparamagnetism* (hence SPM), and is described below.

Superparamagnetism. Added the thermal energy k_BT and with no applied field, the particles have a finite probability to overcome the energy barrier associated with the anisotropy energy KV. This probability can be described by a Boltzmann

distribution of the magnetization flip frequency

$$f = f_0 e^{-\frac{KV}{kT}}, \tag{1.8}$$

where f_0 is the "attempt" frequency and is typically 1 GHz. f_0 also depends on the volume and temperature of the particle as $f_0 \propto \sqrt{V/T}$. Alternatively, $1/f$ can be described in the time domain as the average time between two successful flips. This is known as the *Néel relaxation time*[26]. When the time used to measure the magnetization of the nanoparticles is much longer than the Néel relaxation time, their magnetization appears to be, in average, zero. They are said to be in the SPM state. In this state, an external magnetic field is able to magnetize the nanoparticles with no apparent hysteresis, similarly to a paramagnet, however, their magnetic susceptibility is much larger than of paramagnets, so in that sense they are *super*paramagnets.

Examining equation (1.8) we see that the exponential dependance on the volume and the temperature means that ferromagnetic particles can become superparamagnetic when in small enough sizes and high enough temperatures. For example[27], a spherical iron particle 115 Å in radius whose only source of anisotropy is its first-order crystal anisotropy will have a relaxation time of 0.1 sec at room temperature, while a 150 Å particle will have a relaxation time of 10^9 sec.

Superparamagnetism can be a good tool when used as a magnetic core since it displays no hysteresis. However, at low temperature the Néel relaxation time grows exponentially and spontaneous magnetization flips becomes rare. The temperature where it happens is commonly defined to be such that corresponds to a relaxation time of 100 seconds, that occurs when the thermal energy $k_B T$ is approximately 1/25 of the energy barrier. This temperature is called the *blocking temperature*:

$$T_B = \frac{KV}{25 k_B}. \tag{1.9}$$

When close to T_B, changes of magnetization reorientation occur with relaxation times comparable with the time of a measurement. The result is an observable lag of magneti-

zation changes behind field changes. This phenomenon is called *magnetic after-effect* or *magnetic viscosity*. Well below T_B the thermal agitation can be neglected and static magnetization is calculated by minimizing the total system free energy of equation (1.7). This blocking state leads to hysteretic behavior, which is unsuitable for magnetic microscopy and limits the possible working temperatures.

The common way to measure the blocking temperature is to run a ZFC (zero field cooling) followed by heating back up and FC (field cooling) measurement. The way it is done is as follows, cooling down with no magnetic field to low enough temperature allows for the particles to switch from their SPM state to the blocked state with almost no magnetization – this stage involves no measuring. Then, turning a small field on (say, 100 Oe) and warming up while measuring the magnetization. During the heating, more and more particles will be magnetized due to the field, causing the magnetization to increase until reaching T_B and then the particles will gradually switch to the SPM state lowering the magnetization. Finally, the FC stage takes place, and when below T_B the particles will be blocked at the magnetization reached at T_B. The blocking temperature is determined by the peak in the ZFC and is field dependant. When a stronger external magnetic field is applied, the magnetic anisotropy of the nanoparticles can be crossed at a relatively lower temperature, and hence, the blocking temperature shifts to a lower value.

Table 1.2 below presents the blocking temperatures of nanoparticles that were reported in the literature. We need to keep in mind that such measurements are performed on a cluster rather than a single nanoparticle and each nanoparticle may have a different easy axis, hence such a measurement is an average on the particle's easy axes for magnetization, as well as their sizes. From this table, one can see that the small size does not ensure that the particle will be SPM even around room temperature. Therefore if we are interested in using such particles as a magnetic core for cryogenic temperatures, the choice of particles is of crucial importance. To prove the feasibility of transporting nanoparticles into a nanometric sized and sharp tip any kind of particles can be used as long as they are ferromagnetic and in the SPM regime. In this thesis all the tests were done with magnetite NPs at average size of 6nm (Liquids Research Ltd.), supplied with the courtesy of Prof. Ron Naaman from the Chemical Physics department and the

Tab. 1.2: *Blocking temperature of different nanoparticles*

Material	Size [nm]	T_B [K] measured at H_{FC}=		
		100 Oe	500 Oe	1000 Oe
Fe@Au[28]	5-15	42		
Fe_3O_4[29]	5	110	50	7
Fe_3O_4[30]	4		45	7
Fe_3O_4[30]	11.5		107	
Fe_3O_4[30]	47.7		300	
Co[31]	3.5	170	100	90
$CoFe_2O_4$[29]	5	60	52	46
$MnFe_2O_4$[29]	5	48	40	30
NiO[32]	2	2		
NiO[32]	7	5		
fcc-Ni[33]	30-40	300		
hcp-Ni*[33]	35-40	12		

* hcp-Ni nanoparticles displayed different magnetic behavior in other papers

assistance of his Ph.D. student Tatikonda Anand Kumar.

1.2 Experimental Setup

In this section the methods and experimental setup of a complete fabrication of a Pb SQUID-on-a-tip is described. Also the experimental setup of the measurement system will be presented here.

1.2.1 Tip Processing

The process of making a sub-micron tip is rather simple. The starting point of every tip is a glass (or quartz) tube of any type with an outer diameter of 0.6–1.2 mm and length of 7.5–15 cm. The tube is being cleaned externally with acetone and later with methanol and dried with dry nitrogen gas flow. It is then put in a designated pulling machine (Sutter Instrument Co. P-2000 Micropipette Puller) that employs a CO_2 laser to warm the glass while it is being pulled from both sides. The CO_2 laser emits an IR light at the wavelengths of around 10μm, which most of it is being absorbed by the glass,

and leads to a very efficient heating. The Micropipette Puller is fed with a program that utilizes a number of command lines of 5 parameters each to produce the wanted result (the programming is done in the method of trial and error). The tube is pulled and eventually breaks in a clean way to create two hollow tips of equal diameter.

A program that yields a 250 nm tips of quartz tubes, with an inner diameter of 0.5 mm and outer diameter of 1 mm, is presented in table 1.3 and followed by an explanation.

Tab. 1.3: *Sutter Micropipette Puller program*

	Heat	Filament	velocity	Delay	Pull
Line 1	750	5	25	128	118
Line 2	600	4	40	128	60
Line 3	650	4	60	127	75

The five parameters are:

- Heat - a number between 0-999 that specifies the laser intensity and consequently the amount of energy supplied to the glass.

- Filament - specifies the scanning pattern of the laser beam, each of which defines the longitudinal length and rate of the scan. 5 is equivalent of 8 mm wide scan and 4 is for 6.5 mm scan.

- Velocity - a number in the range of 0-255 that defines the velocity the glass carriage moves during the initial pull (pull due to permanent weights) before the hard pull is executed.

- Delay - a number between 0-255 that times the hard pull start relative to the laser deactivation. 128 means that the laser is deactivated at the same time that the pull is started. Lower(higher) number than 128 means that the laser is deactivated after(before) the pull was started.

- Pull - a number in the range of 0-255 that defines the force of the hard pull.

1.2.2 Pb SQUID Fabrication

A SQUID should consist of two superconducting (SC) leads that are connected to a SC loop with two weak links to it as further explained in section 1.1.2.2. The procedure of producing a SQUID on a sharp quartz tip consists of evaporating a SC metal on three sides of the tip at the proper angles and parameters for each metal and tip size. The tip's apex is evaporated with smaller thickness, so that its smaller thickness, together with the different substrate texture and smaller width, naturally creates the two weak links (general constriction weak links). An illustration of how the Pb SQUID tips are made is presented below in figure 1.4.

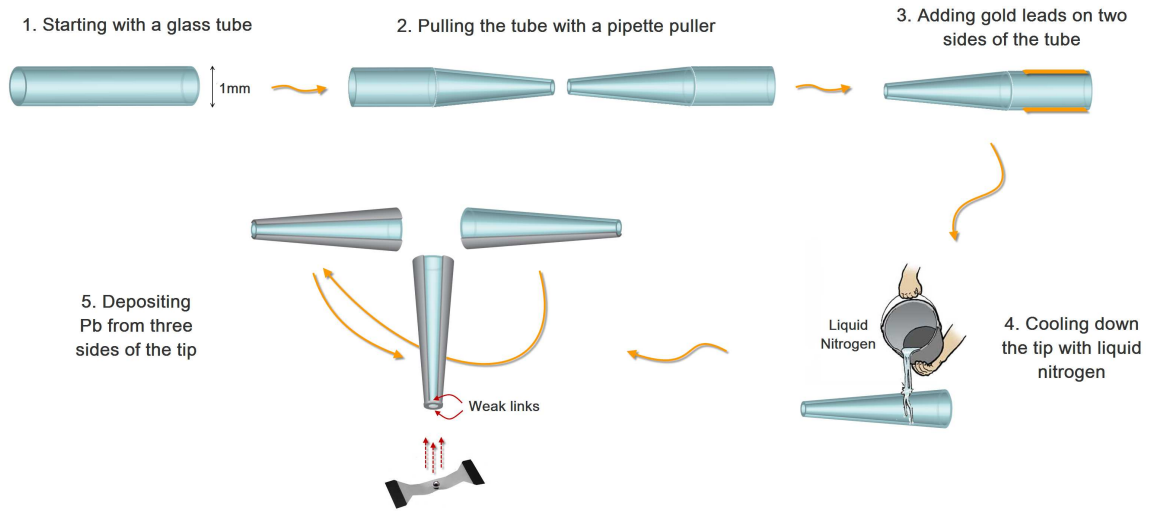

Fig. 1.4: *Illustration of a Pb tip production.*

The chosen SQUID's metal for measuring the nanoparticles effect was lead (Pb). The lead was taken for its higher critical temperature property (7.2K) which enables us to work with a much less complicated cooling system - namely dipping a probe into a liquid Helium (4.2K) dewar (see section 1.2.3.1 ahead for more details). This higher measuring temperature is also very important for minimizing the nanoparticle's blocking temperature effect. From our experience, another beneficial aspect of Pb tips is their slower oxidation rate.

Lead, in contrary to other SC metals (as Al, V, Nb), is highly kinetic at room temperature. When thermally evaporated on a room temperature substrate it flows to create

islands of lead that will or will not percolate depending on the thickness of evaporation. For this reason the substrate has to be cooled down as much as possible before evaporation. However, due to the low thermal conductance of glass and its conical tip, it becomes harder to implement. Cooling is done with two cold bodies, that are as adjacent as possible to the tip, connected with a copper thermal braid to a cup filled with liquid nitrogen. In addition the vacuum chamber is kept in some exchange gas pressure (between $10^{-5} - 5 \cdot 10^{-5}$ Torr) for 45–50 minutes.

1.2.3 Measurement Setup

Measuring a fine and delicate SQUID is not a simple task. It involves having a non interfering and very sensitive reading electronics and devices, and also protection mechanisms for the SQUID to protect it from electrical spikes and static charges. To succeed in that, a measurements probe was designed and built to fit the requirements. The electronic measurement devices and electronic circuits will be presented here as well in their functionality level.

1.2.3.1 The Probe

The probe is designed to be lowered into a liquid He dewar, while the sample tip is kept in low vacuum (with some exchange He gas). In figure 1.5 (a), the left side (green) is made of G10 (glass fibers in an epoxy matrix) to electrically isolate the tip from its surroundings (marked as 1). On it there is a female "dovetail" socket to attach a male tip holder or detach easily (2). This part is connected to a diode thermometer and a resistance heater to control the temperature near the tip if needed (3). Further to the right is the electronics breadboard for all the electrical circuitry in the probe (4). It was planned as a breadboard, which can quickly be removed, since it allows for easy changes and additions to it on the fly. On the board an optical relay (5) was placed to short the tip's electrodes and minimize the risk of being burned while moved and while working on the board. More to the right, protected from magnetic fields by a "sandwich" of Niobium–Mu-metal–Niobium cylinder (6), is the PCB board of the SSAA chip (SQUID Series Array Amplifier) fabricated at

NIST[34], which is a cryogenic current amplifier. This chip is comprised of a hundred SQUIDs in series that are inductively coupled to the current from the SQUID-on-tip and to another feedback coil. The current in the SQUID coil is transformed to voltage on the SSAA. The cylinder above the probe is its vacuum cup (7), which encloses the whole probe and vacuum seals it.

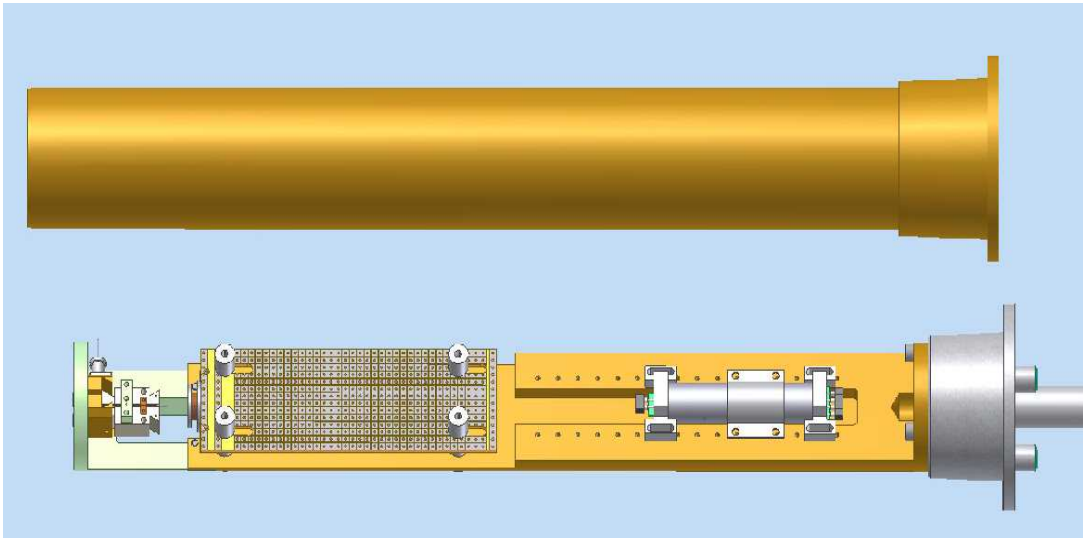

(a)

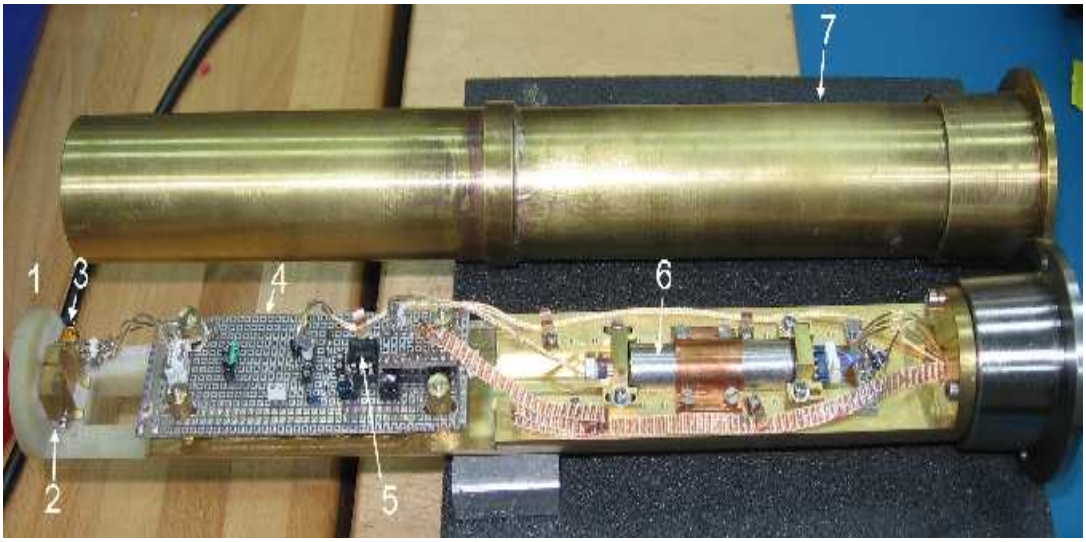

(b)

Fig. 1.5: *(a) The probe's design; (b) A picture of the probe including the electronics breadboard and the wiring. The upper piece in both of the images is the vacuum can.*

1.2.3.2 The Measurement Devices

The electrical scheme presented here in figure 1.6 shows the circuit of the breadboard as well as the outer (room temperature) electronic boxes. For detailed information on the circuitry of the feedback and preamplifier boxes see appendix A. The 4 Ω resistor is the shunt resistor, thats sets the voltage bias of the SQUID and reduces the hysteresis in the SQUID's I-V curve. The 5 kΩ resistor and the 10 μH inductor are used to reduce the current flow through the SQUID to the μA-mA regime and to prevent high frequency spikes respectively. The relay is a VO14642 Vishay optical relay that can be only used above -40 °C and is an open circuit at the working temperature.

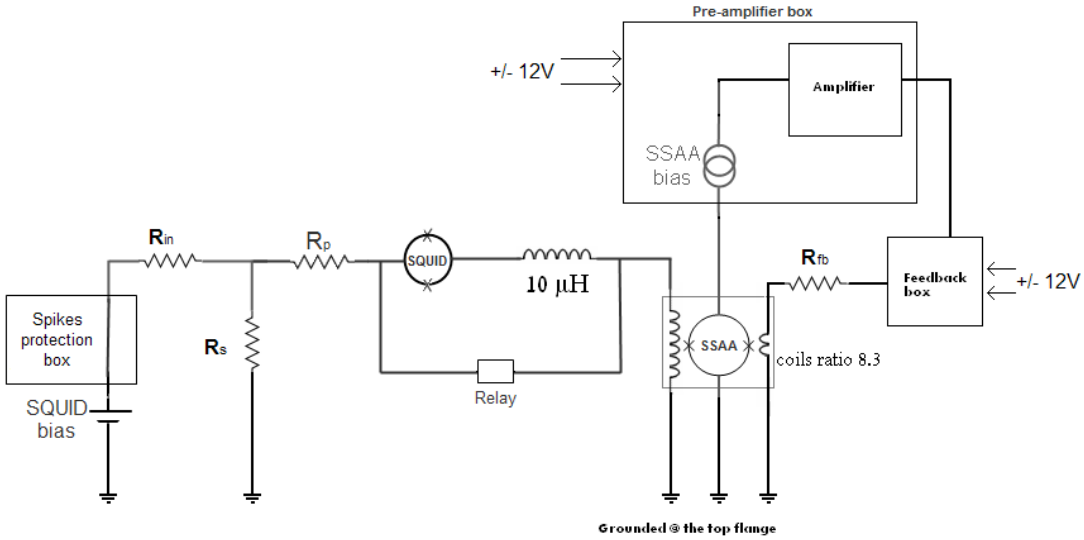

Fig. 1.6: *Simplified measurement circuit. Here, R_{in} is the input resistor, R_s is the shunt resistor, R_{fb} is the feedback line resistor and R_p stands for parasitic resistance, which is the inherent line and contact resistance of the SQUID line.*

The SSAA is comprised of a hundred Nb SQUIDs in series, each with JJs of Nb/AlO_x/Nb. The SQUIDs are inductively coupled to a coil, situated on the SQUID-on-a-tip line, and a feedback coil with lower amount of windings (the coils calculated ratio is 8.3). When the feedback loop is closed, current in the SQUID-on-a-tip line creates a magnetic field in the SSAA, which the feedback coil acts to cancel. Because of the winding

ratio, the current through the feedback coil needs to be 8.3 times larger than that of the SQUID-on-a-tip, making the SSAA a cryogenic current amplifier.

The pre-amplifier box has three main purposes. One is the current biasing of the SSAA to put it in a sensitive working point. The other and most important is to amplify the SSAA signal (which reads the SQUID) in order to improve the SNR. The third use of this box is to "zap" the SSAA. Zapping is necessary when a magnetic flux is trapped in the SSAA, which can happen when cooling down while applying field or using currents in the SSAA that exceed the critical current. It is done by applying enough bias current in the SSAA to warm it to the normal state and release the trapped flux.

The feedback box is in charge of giving feedback to the SSAA through the feedback coil. Its purpose is to compensate for changes in the magnetic field on the SSAA, due to changes of the tip's current, allowing the current through the SQUID to be tracked. The feedback voltage is proportional to the SQUID-on-tip current and acts as the output signal. Implemented in the circuit are also a gain and bias knobs to assist the locking of the feedback box.

Both boxes are powered by two 12 Volts batteries to avoid additional electrical noise of the mains power line and also avoid grounding issues.

Magnet. For controlling the magnetic field we use a SC magnet which sits inside the dewar. Its field to current ratio is 1119 G/A and can supply fields as high as 5.5 Tesla.

Other devices such as a SQUID protection box against spikes that come from connecting or disconnecting wires and also to slowly turn the voltage on the SQUID were assembled. Another protection box was made in order to be able to measure the tip resistance indirectly at room temperature without passing dangerous currents through it.

Multimeters, Power suppliers and Oscilloscope. The measurement system included some additional electronics:

- Three Yokogawa 7651 voltage/current sources. One supplies current to the thermometer diode, another controls the SC magnet power supply and the last is used for voltage bias of the SQUID.
- A Toellner 8751 power supply to control the magnet's current.
- A Tektronix TPS 2014 oscilloscope, for monitoring the feedback locking.
- An HP 34401A digital multimeter (DMM) to measure the feedback voltage A.
- A Keithley 182 sensitive digital voltmeter that reads the voltage of the thermometer diode.
- An Agilent 8904A multifunction synthesizer to add modulation on the input signal to the feedback coil, for spanning the SSAA response.
- A self-assembled distribution box for the thermometer, heater and relay wires.

Software. The software used to measure and control these devices was Labview. Matlab was used for data processing and to produce graphs.

2. Goals

The goals of this thesis are:

- Prove the feasibility of fabricating a tip filled with a magnetic core material.
- Successfully fabricate a SQUID on a tip filled with a magnetic core material.
- Measure and characterize the above tip.
- Integrate the new tip in the existing microscope (long term).

3. Results

This chapter will be separated into four sections. Three different attempts that were done in order to add a metallic core for the SQUID via:

- Pulling wires together with the glass tubes.
- Attempts of chemical nickel plating of the tubes.
- Capillary filling of tips with magnetite nanoparticles.

The last section is dealing with the production details and results of the Pb SQUIDs.

3.1 Wire Pulling

A thin (25–50 μm) wire is inserted into a tube and then put in the puller making sure that the wire is free. The pulling is done generally in 3 steps. Step 1 – pulling the tube to reach an inner diameter that is slightly larger than the wire's diameter; step 2 – heating the tube, while holding the puller weights such that there is zero applied force on it and it is not pulled at all. This step is done in order to make the glass reach a good mechanical grip and thermal connection with the wire; step 3 – continuing the pulling to the break in the desired way.

Most of the work was done in this area, since if it were successful, the wire, which plays the role of a flux amplifier for the SQUID, could also be used as an STM scanning needle for surface probing. STM needle will make the use of a tuning forks unnecessary and also can give more information on the surface. Attempts to accomplish this goal included:

- The use of different type of glasses (quartz and borosilicate glass) which have different softening and working temperatures.
- The use of different tube diameters and wall thicknesses.
- The use of different metal wire materials (SS 430, Invar, Pt, Ni 270).
- The use of different metal wire initial diameters.
- Utilizing heating of wires while pulled by applying current.
- Testing hundreds of pulling recipes of the micropipette puller.

When being pulled, the glasses and metal wires are heated to temperatures, where the glass is workable. To get a better feeling about the working temperatures, table 3.1 lists the materials used and their typical temperatures. For glass and quartz we note the softening point and the working point, and for metals their melting temperatures. The working range of glass is defined to correspond to a viscosity range from the working point to the softening point ($10^{7.6} - 10^4$ Poise). Simply put, it is that range of temperatures that corresponds to the range from where glass just begins to soften up to the point where glass is too soft to control.

Tab. 3.1: *Softening, working and melting temperatures of glasses and wires*

Material	Softening point [°C]	Working point [°C]	Melting point [°C]
Quartz	1710	n/a	-
Borosilicate glass	821	1252	-
SS 430	-	-	1427
Invar	-	-	1426
Nickel 270	-	-	1454
Platinum	-	-	1768

The first thing noted was that the quartz tube, which needs higher laser intensity to get it to its working temperature, heated the wires until the wire melted every time even for platinum wire which has a melting temperature of 1768 °C. The quartz softening temperature is around 1710 °C. However, the quartz is heated to a higher temperature

than that while being pulled, which causes the wires to melt on the first pulling step. Quartz tubes were ruled out for this reason.

During all of those aforementioned attempts, few problems always arose. First was the breaking of the wire to segments in few places along the pulled area instead of continuous stretching. This happened in most of the attempts to pull wires with the glass tubes for all the magnetic wires that were examined. An extreme example can be seen in figure 3.1 (a),(b). We believe that stretching can be achieved with some materials and not with others, depending on their ductility at the pulling temperature. Of the above materials for wires, only Pt was successful with the aid of Sofia Kokotov from the Nanonics Imaging Ltd. lab, which has many years of experience with wire pulling. Out of the remaining three only the stainless steel wires showed some stretching, up to about 40% of their initial diameter (see figure 3.2 (a)). Platinum is known as a good candidate for pulling (it is commercially sold[1]), but its downside is that it is not magnetic and therefore it can be tested as an STM tip but cannot be used as a flux focus. Figure 3.2 presents the best results achieved so far with the stainless steel and platinum wires. However, pulling Invar and Ni 270 wires proved to be unsuccessful every time again, even with Sofia's assistance.

A second phenomenon that was encountered is air bubbles in the glass along the heated area of the tube (see figure 3.1 (b)). Bubbles might come from air that was trapped between the wire and the tube in the wire grip stage of the pull, and starts to penetrate the glass when it gets softer. This phenomena causes the tip to break at certain weakness point of the tube instead of being broken naturally at the center. Overcoming this difficulty is done by using slightly lower heat parameter (lower laser intensity) during the second stage of the pull (recall section 3.1), which is not hard to do. However, this limits us on the heat parameter in the final pull (third step) as well.

3.2 Plating

In this method there were two main ideas that were tested. The tube's interior nickel electroplating prior to the pulling and nickel electroplating a tip after pulling a platinum

1 www.nanonics.co.il

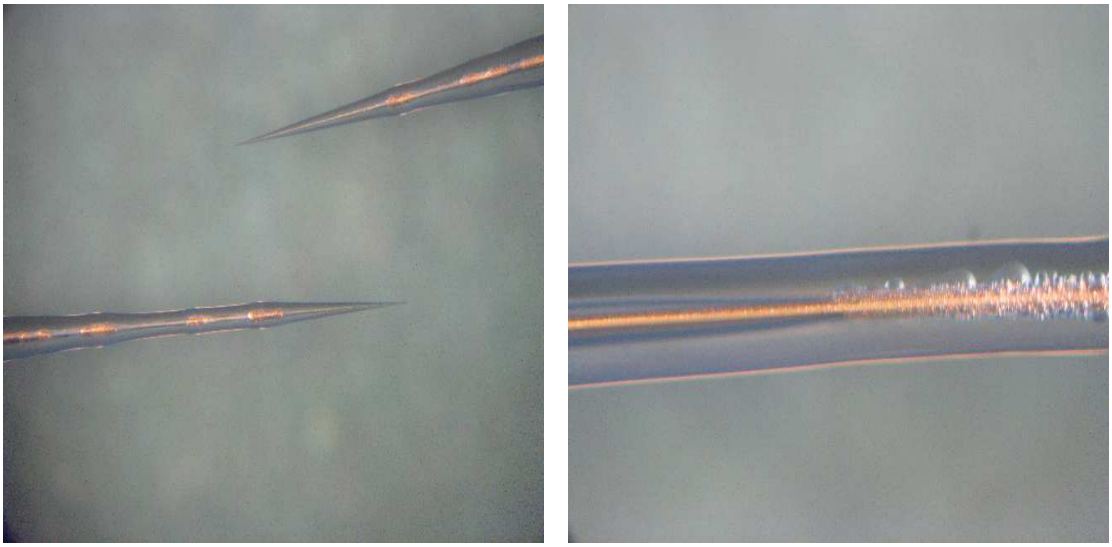

(a) (b)

Fig. 3.1: *(a) Tearing effect of wires; (b) Bubbles phenomenon.*

wire inside a tip, as explained in section 3.1.

For plating the tube's interior, the first step is creating an electrode on the tube interior to have a preferred nickel growth location. This was done by making a silver electroless plating solution (mixing Tollens' reagent $Ag(NH_3)_2(aq)$ and Glucose $C_6H_{12}O_6$) and putting the tube in the solution. The small inner tube diameter capillary pulled the solution up above halfway along the tube. After 10 minutes in the solution the tube interior is silver plated and can serve as an electrode for nickel electroplating. The chemical reaction of the silver electroless plating is:

$$[Ag(NO_3)_2]^+(aq) + e^- \rightarrow Ag(s) + 2NH_3(g). \tag{3.1}$$

Cleaning procedures. Silver plating was tested with three different cleaning procedures to determine which achieve the best adhesion of the silver to the quartz. The cleaning methods were: Chromic acid, partial RCA and HNO_3-NaOH. Chromic acid is a powerful oxidizing agent and is a useful compound for cleaning laboratory glassware of any trace of organic compounds. It is prepared in situ by dissolving potassium dichromate in concentrated sulfuric acid, which is then used to wash the apparatus. The RCA clean

is a standard set of wafer cleaning steps, that is used to remove organic contaminants, oxides and ionic contaminations. The cleaning procedure of the tubes was the first RCA step (SC-1)- the organic contaminants removal by a mixture of NH_4OH:H_2O_2:H_2O in ratio of 1:1:5. The HNO_3-NaOH cleaning is composed of two baths- acidic bath (nitric acid) to remove of inorganic deposits and an alkaline bath (sodium hydroxide) to dissolves grease, oils and fats. In all three methods the tubes were dipped in a $SnCl_2 \cdot H_2O$ surface activator (0.1-0.5%) for few seconds and later cleaned with dry N_2.

After putting three tubes, cleaned by each of the above methods, in the silver electroless plating solution the results showed some differences as can be seen in figure 3.3.

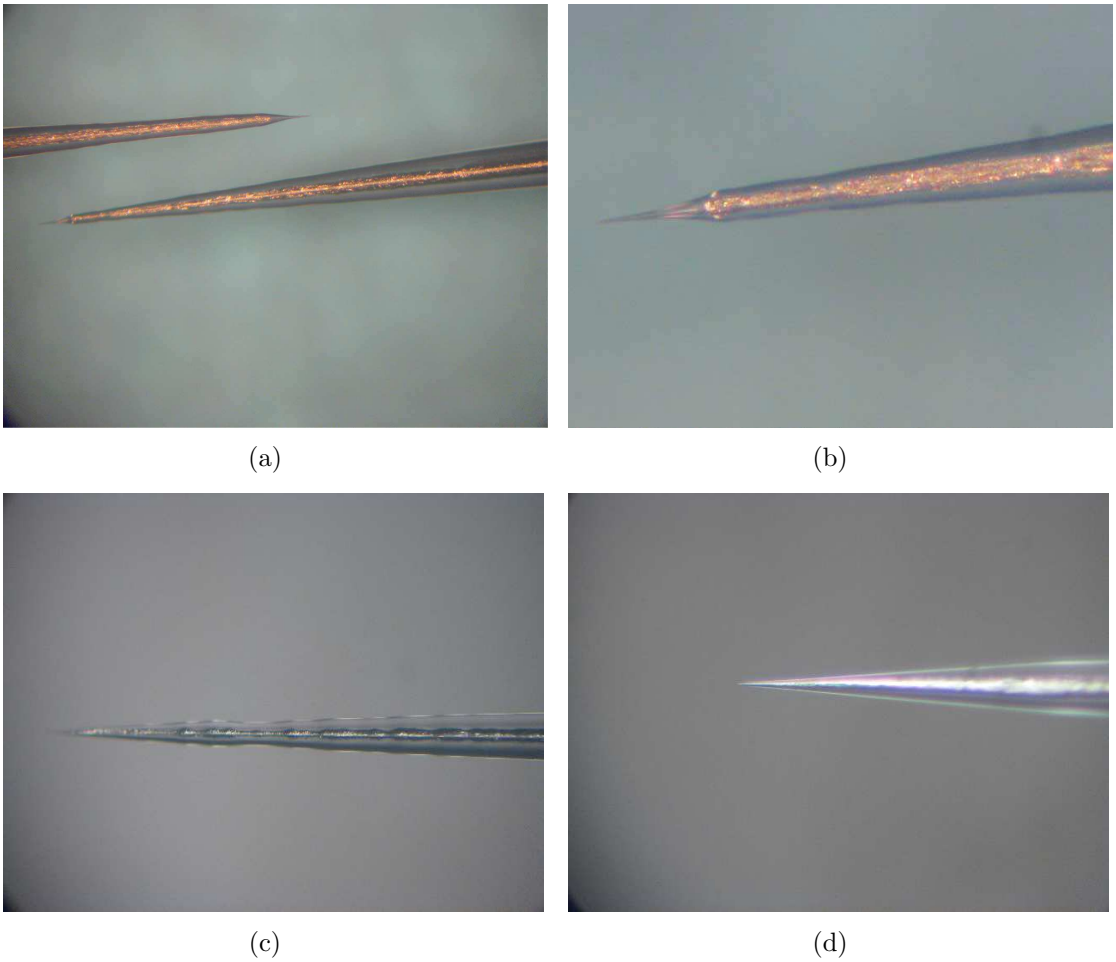

Fig. 3.2: *(a) A quartz tip pulled together with a 430 stainless steel wire; (b) Magnified image of (a); (c) A quartz tip pulled together with a Pt wire*; (d) Magnified image of (c)*

* The Pt tip was made by Sofia Kokotov and Aaron Lewis of Nanonics Imaging Ltd.

Clearly the HNO_3-NaOH method did not clean well enough. The RCA seemed to do the best job, perhaps because of bubbles flow through the tube, and was used from then on.

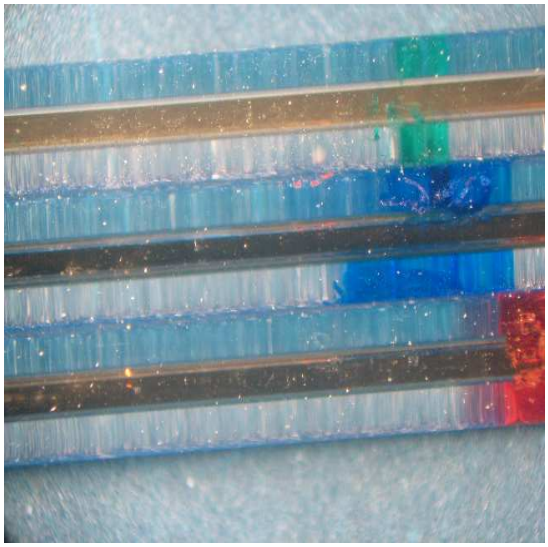

Fig. 3.3: *Cleaning comparison after silver plating of the inside of quartz tubes. Green (upper): HNO_3-NaOH. Blue (middle): RCA. Red (bottom): chromic acid.*

Nickel Sulfamate and nickel sulfate were the chosen reactions for the nickel plating process since both are in wide use in the industry. The solutions were made according to table 3.2 and heated to roughly 50°C. The silver plated tube served as a cathode while a nickel stripe as an anode. In order to keep a fresh supply of Ni ions in the tube, the tube was pumped with a syringe to create a flow.

Tab. 3.2: *Nickel electroplating solutions*

Method	$NiSO_4 \cdot 6H_2O$	$Ni(SO_3NH_2)_2$	$NiCl_2 \cdot 6H_2O$	H_3BO_3	Temp. range [°C]
Nickel Sulfate	225–400	-	30–60	30–45	32–60
Nickel Sulfamate	-	300–450	0–30	30–45	44–66

All amounts are in [g/l]. The numbers are taken from reference [35]

Few issues arose while doing the nickel plating tests that made it unusable. One difficulty was the small plated area of the tube. The nickel was deposited on the end of silver electrode and grew to seal the tube for liquids flow. The flow is essential since Ni^{2+} ions need to be replenished while electroplating or else the chemical reaction will cease. The deposited area was too narrow for us to be able to align it exactly in the middle of

the puller laser beam. Moreover, we have noticed that the nickel solutions damaged the silver plating adhesion. The adhesion of the silver was tested with water by running a flow of water through it and the silver held strong to the walls. However, when used with the nickel solution it quickly pulled all the silver from off the walls.

The second idea of electroplating was to first pull a platinum wire in a tip and then let the Ni grow on the tip's sharp edge over the Pt metal and be a small magnetic core on the end of the Pt wire. This was done in a similar way to the electroplating explained above, but with a smaller current. The two electrodes were a Ni stripe and the Pt wire in a tip, whose end was held in a Nickel Sulfamate solution.

This was possible to grow nickel at the tip, but due to the submicron size of the tips and the different geometries of the pulled platinum tips (in some, the wire reached the tip's apex and in some it was hidden deeper in the tip), the process was hard to control. Furthermore, oxygen and nitrogen bubbles are created during the plating, blocking the ions flow and are released from the tip once they are big enough, making room for another bubble to grow. A bubble sitting on the tip makes the process very slow and when it is released, many ions reach the Pt electrode and the process in more rapid. This makes the plating rate very unstable. An image of such a tip, which was left few seconds more than it should have can be seen in figure 3.4.

Fig. 3.4: *Grown nickel on the end of a platinum wire tip.*

3.3 Capillary Fill with Nanoparticles

Capillary action is the action in which liquids spontaneously (meaning with no applied external force) rise in a narrow space such as a thin tube. If the diameter of the tube is sufficiently small and the adhesion to the walls is stronger than the cohesive forces between the liquid's molecules, the liquid will rise in the tube until an equilibrium is reached.

The nanoparticles are in a dense solution of paraffin oil which is quite viscous. Therefore it is being diluted with 200 μl of toluene for every 3 μl of the original solution. The oil and toluene isolate the particles from one another to prevent the nanoparticles from clustering, but when adding ethanol it enables the clustering and also helps adhesion to the glass substrate of the tubes.

The first attempt was to create a thick layer of nanoparticles from within the tube and later pull it to a small diameter tip, very similar to the idea of the Ni plating prior to the pull. A diluted solution that contained ethanol was made and a quartz tube dipped into it. With a strong magnet the particles were manipulated to stick to the walls of the tube at the center point and then the clear liquids were carefully sucked out with a syringe.

The result of plating nanoparticles inside a tube was a small length magnetite tube grown inside the quartz tube. This magnetite tube proved to be brittle and to have weak adhesion to the walls. Figure 3.5 (a) shows what happened when the tube was put again near a magnet after it was dried. Such an unbroken tube was put in the puller, but it took much larger amount of heat to pull it and the result, as can be seen in figure 3.5 (b), was a severe damage to the tube.

A different attempt with nanoparticles was to have the magnetite solution raised by the capillary force to the top of a readily pulled tip. However, in the case of an extremely sharp tip the capillarity will be suppressed earlier on the rise since the air that exists in the tube has a limited flow outside the sub-micron cross-section of the tip's opening.

To overcome this difficulty quartz tubes with quartz filament attached to it from within were used (see figure 3.6 (a)). In those tips the capillarity occurs near the filament. When the wide side is put in a liquid, the liquid climbs up the filament to the top of the

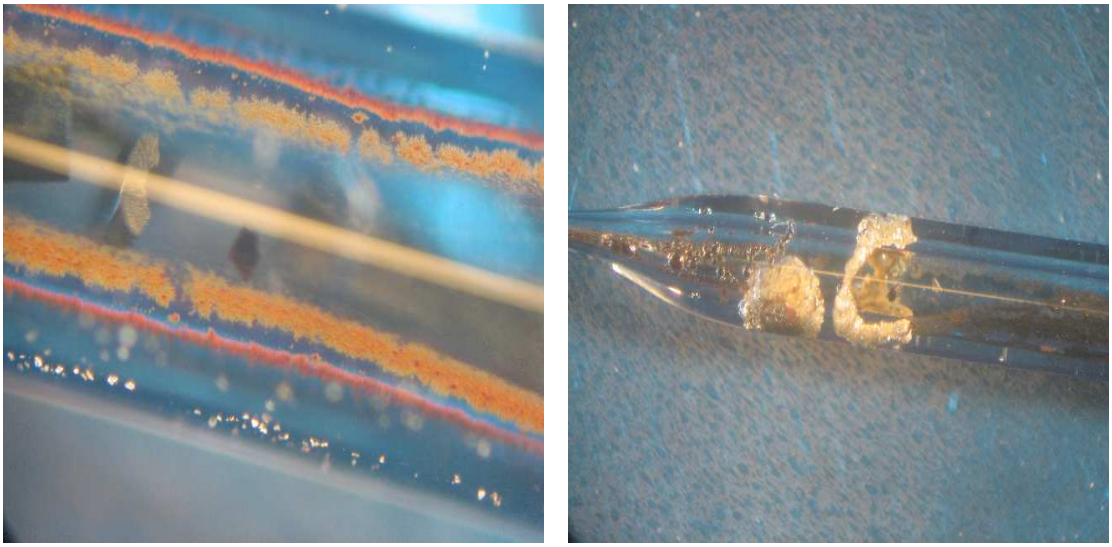

(a) (b)

Fig. 3.5: *(a) A broken plated cylinder of magnetite nanoparticles; (b) A typical pull of such plating.*

tip and starts to fill it downwards (see figure 3.6 (b)).

In order to transport the nanoparticles to the tip, they are diluted with 200 μl of toluene for every 3 μl of the original solution as before. Then the tip's wide side is put in the solution for a few seconds until the top of the tip is filled. Now that the tip is filled, it should be dried out of toluene. This is done in two steps: First, putting the bottom side of the tip in toluene for an hour in order to have a higher vapor pressure of toluene inside of the tube than on the outside (in the tube the equilibrium vapor pressure of toluene is assumed to be reached), ensuring that most of the evaporation will occur at the tip's sharp end and perhaps leave particles attached to the walls while doing so; second, holding the tip in air for another hour to let it dry completely and leave only the particles.

Tips that contained filaments embedded in them were pulled to an outer diameter of approximately 250nm, then filled with different levels of particle dilutions and dried as explained above. Later they were deposited with thin aluminum layer of 25nm from three sides (for resolution and contrast of images) and imaged by a SEM. All of the tips have shown some degree of filling. In figure 3.7, a perfectly filled tip next to a broken tip that

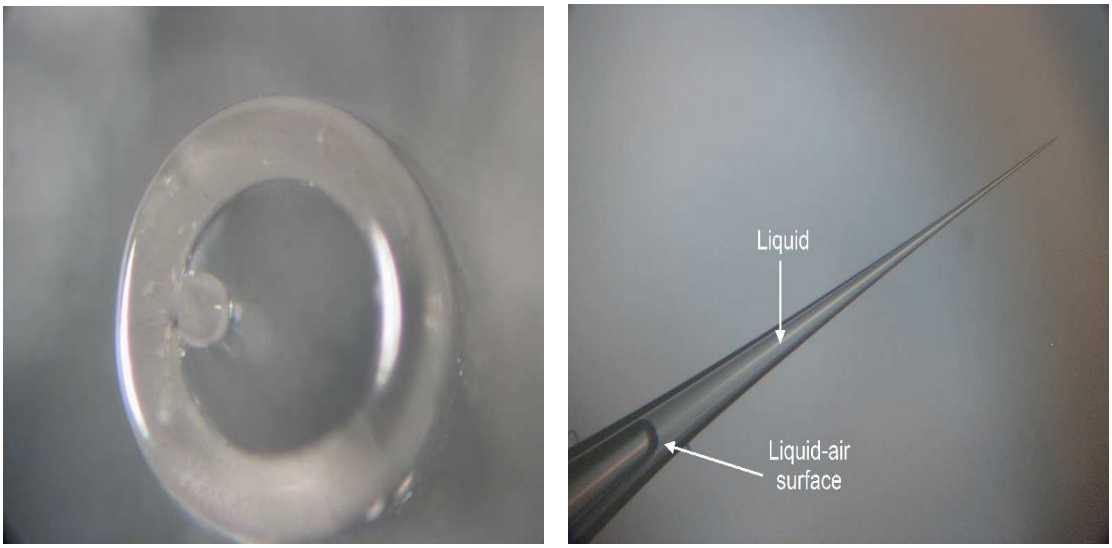

(a) (b)

Fig. 3.6: *(a) Cross section of a quartz tube with a filament; (b) Water filled tip (with filament).*

was filled without knowing it was broken is presented. The broken tip seemed completely filled as well in spite of its much greater inner diameter.

3.4 Pb SQUID Tips

Fabricating a working Pb SQUID tip is a crucial step towards measuring how a tip with nanoparticles improves the magnetic sensitivity of the SQUID. After showing that a tip can be filled, what is left is to measure the same SQUID's current to flux characteristics with and without the core.

Much time and many resources were spent in order to bring the lead tips fabrication to a good success rate. There seem to be two related problems with the lead tips. The first is a poor adhesion of the lead to the quartz tip substrate (see figure 3.8 (a)). A better adhesion is achieved by using low oxygen pressure ($10^{-6} - 10^{-4}$ torr) inside the vacuum chamber while evaporating. However, when the adhesion is improved, crystals are emerging on the lead especially in the vicinity of the tip's apex and on it (figure 3.8 (b)).

Many attempts to improve the adhesion to the quartz have been made, including the

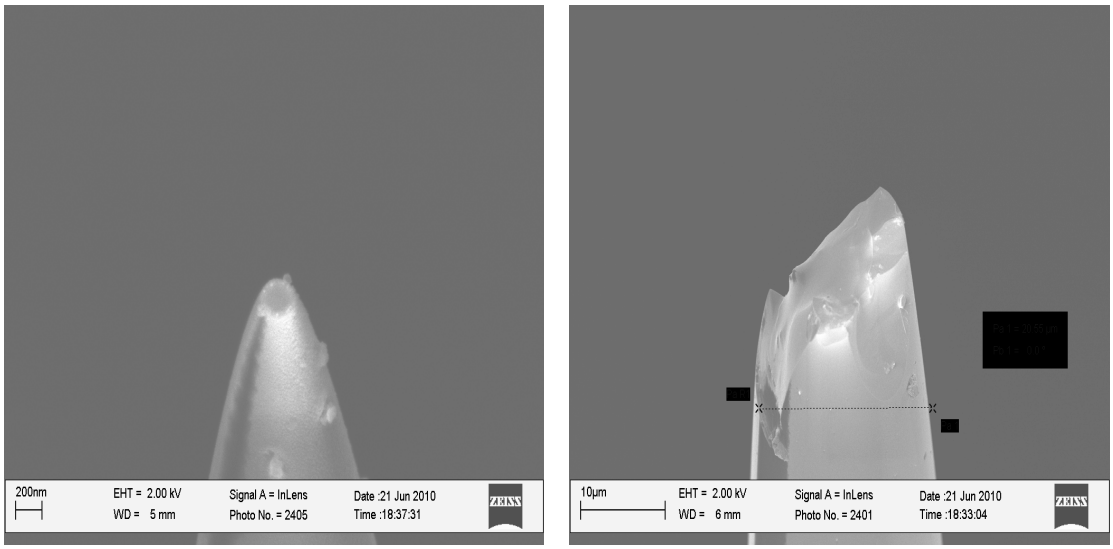

(a) (b)

Fig. 3.7: *(a) A quartz tip filled with magnetite nanoparticles evaporated with aluminum from 3 sides; (b) A filled broken tip with inner diameter of few microns.*

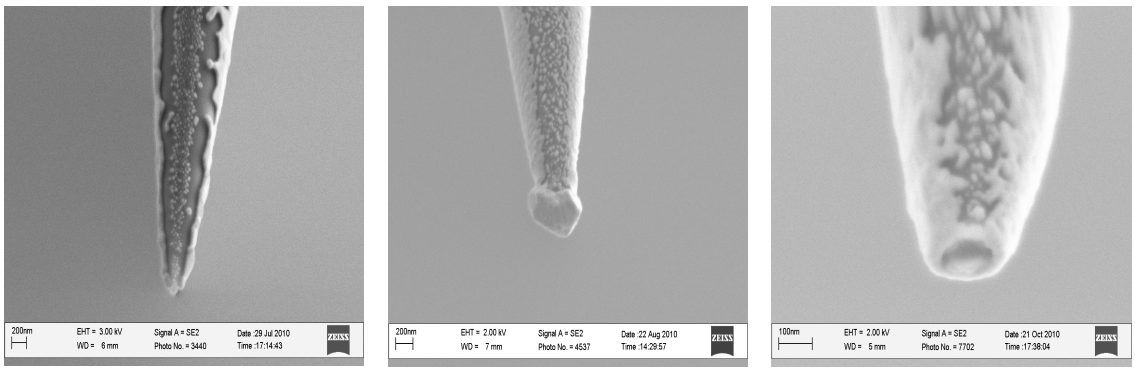

(a) (b) (c)

Fig. 3.8: *SEM images of Pb coated tips. (a) A tip with bad adhesion; (b) A tip with better adhesion but with a crystal blocking its apex; (c) The wanted result.*

implementation of high voltage electrodes to create O_2 and CF_4 plasma in the chamber, an intermediate layer of other materials (such as vanadium, chromium, aluminum and lead oxide) and the use of clean air (low oxygen pressure for adhesion purposes, with nitrogen as the exchange gas). None of the above showed consistent results for adhesion improvement except the oxide intermediate layer that seemed to improve the adhesion

but still created crystals once in a while.

These crystals seemed to appear rather randomly, but always with the presence of a good adhesion to the glass (oxygen was always involved), leading us to consider two possible scenarios- either the crystals were growing on the tip in the presence of lead and oxygen to create some crystalline oxide, or the crystals are present in the chamber (from an unknown source like the thermal evaporation boat or other) but we see them only when the adhesion is good so they can stick to the tip.

Before having enough statistics on those crystals, the assumption was that maybe water was freezing during the cooldown of the tip. To get rid of ice we have employed several techniques, such as tilting the tip sideways while cooling it, adding methanol to the tip to dilute the water and then warm the chamber up with a cartridge heater to evaporate it. All of the above did not help much, but rather complicated the process and consumed more time.

The oxygen cylinder was replaced with a super clean one (5N oxygen) to exclude some other gases that may freeze on the tip or just dirt in the cylinder. Also the thermal evaporation boat was replaced by a new one to exclude the release of crystals from it and most of the parts in the chamber were cleaned from remnants from old depositions. After all this effort crystals are still emerging once in every third tip on average, suggesting that these crystals are not dirt, but rather lead oxide crystals.

Due to those problems above and the sensitivity of the SQUIDs to electric discharge, which "burn" them easily , up to date, only two working Pb SQUIDS were successfully deposited on tips with filament and measured once. An I-V-H (SQUID's current I_{SOT} - bias voltage V_{in} - Magnetic flux H) graph of one of the SQUIDs is presented in figure 3.9 (a). Both of the SQUIDs did not survive a second cooldown to measure them with nanoparticles magnetic core.

An explanation on the I-V curves. We voltage bias the SQUID and read the current through a coil in the SSAA. At low voltages we see the linear dependance of the I-V curve due to the circuit resistance (mainly R_{in}). At a voltage slightly higher than the value corresponding to the critical current, there seem to be a negative resistance. In fact, this

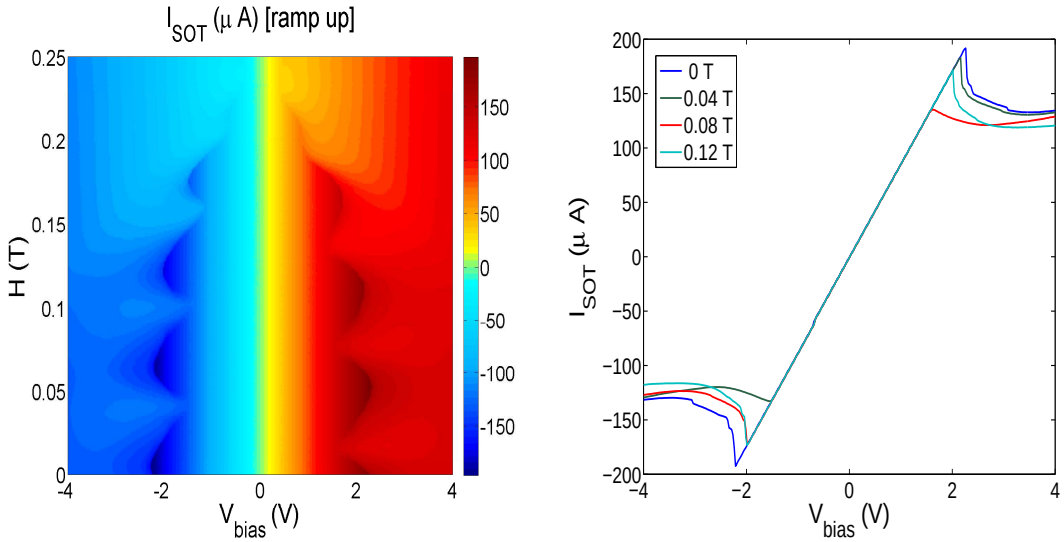

(a) (b)

Fig. 3.9: *(a) A SQUID I-V-H 2D scan showing the critical current oscillations in field until they die out at around 0.25 Tesla. (b) Four I-V cross-sections of (a) at different magnetic fields*

negative slope is an inherent averaging of high frequency Josephson oscillations (the AC Josephson effect) by the measurement system, that cannot resolve them.

In figure 3.9 (a), one can see the critical current oscillations (bias voltage as a function of field) until they die out at about 0.25 T. One would expect, according to the theory, that at zero field the critical current will be maximal and oscillate with field as an absolute value of a cosine, as equation (1.4) indicates. However, a shift of the cosine maximum can clearly be seen here at positive bias voltages, as well as an angular tilt in the cosine shape. This shift is also asymmetric regarding the oscillations at positive and negative bias voltages. The cause of the asymmetry and tilted shape is the fact that both arms of the SQUID were not created equally, as was assumed in the theoretical explanation, but have different inductances and critical currents. Asymmetric SQUIDs were treated theoretically by Fulton et. al.[36], who predicted such behavior.

The SQUID's maximal current, I_m, was calculated at a field of 50 G at a negative voltage of 2.3 V, which meets the maximum of the oscillating critical current curve, and is approximately 200 μA. This critical current is true up to a factor of 2 error.

The periodicity of the maximal current in the field, explained earlier, is of ϕ_0. This

periodicity enables us to calculate the effective diameter of the tip. If one period has a field difference of approximately ΔB=0.055 T, then the calculation, presented below, will give a diameter of 219 nm. This value fits nicely the SEM images of this tip (see figure 3.10).

$$\begin{aligned} S &= \frac{\phi_0}{\Delta B} = \frac{\pi d^2}{4} \\ d &= \sqrt{\frac{4\phi_0}{\pi \Delta B}} = \sqrt{\frac{4 \cdot 2.068 \cdot 10^{-15}}{\pi \cdot 0.055}}\ [m] = 219\ [nm] \end{aligned} \tag{3.2}$$

Where, S is the effective SQUID loop area and d is its diameter.

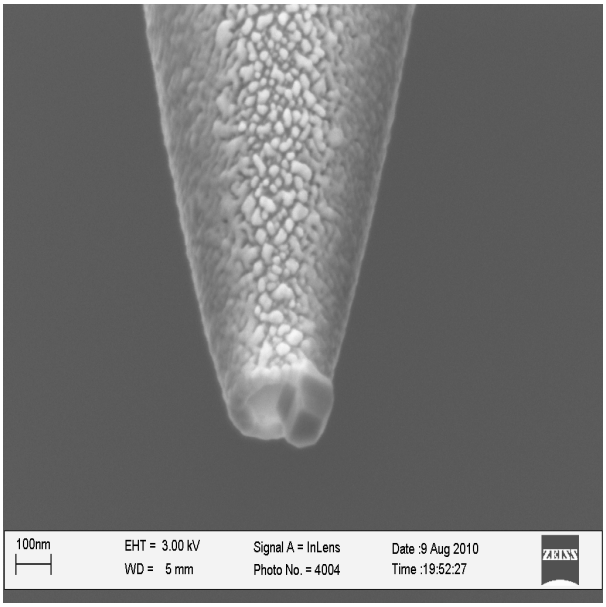

Fig. 3.10: *SEM image of a working Pb SQUID-on-tip, although a crystal can be seen on its apex.*

4. Discussion

From all the methods used to add a magnetic core to the existing SQUID-on-a-tip, the method which was most disappointing was the wire pulling, since it held a great potential for flux enhancement as well as an STM capability integrated to the microscope. A long time was spent in the wire pulling process mainly because there are so many free parameters to tune, like the glass tubes and the wires used, their dimensions and the puller parameters. The magnetic materials that were tested showed a brittle behavior while being pulled and it seems like a very careful choice of materials (and their melting temperatures relative to the glasses' temperatures) could eventually be successful. However, we have decided to give up on this direction since it could take quite a long time with a big uncertainty about its success probability.

The method of plating was tested for a short while with poor results. The attempts to plate the tubes with nickel from within were unsuccessful due to the poor adhesion to the tube. Tubes plated with magnetite nanoparticles had to be pulled with very high laser output power that damages the tubes as well.

Some positive results came from the nanoparticles direction. We have been able to fill sub-micron tips with these nanoparticles and dry them such that the particles stayed on the edge of the tip. A broken tip that was accidently filled showed a promising result– an opening of about 10μm was completely filled (figure 3.7). This complete filling and a partial filling of other tips with more dilute NP solution was reproducible.

The way to measure its contribution to a SQUID sensitivity was to have a SQUID tip, measure its $V(\phi)$ characteristic period and then add the core particles and remeasure it. A first expected difference will be that the period between the field oscillations will become smaller, since the flux passing through a ring of the same diameter will be enhanced and

a period of ϕ_0 will be achieved at lower applied field. Another difference will arise after the first field scan, when hysteresis most probably will appear. The time between the production of a SQUID and the time of its second measurement is in the order of a day or more. For that reason, in addition to its higher critical temperature (as explained in section 1.2.2) Pb, which is less sensitive to oxidation in atmosphere than our Al tips, was chosen to be the material for the SQUID.

The downside of the Pb choice is the bigger difficulty of deposition. Some obstacles were met during this stage– bad adhesion and crystallization on the tip. Solutions that helped the adhesion problem also created more crystal in general and vice versa. Other solutions to those problems are still under examination, but up to date Pb tips are not a stable procedure. In addition to the unsatisfactory success rate of the Pb SQUIDs there was another difficulty. All the tips were examined using an SEM and later on their resistance at room temperature was measured using special circuit. Those tips which failed the two tests were disposed of, but even some of those which seemed to have a good potential to be a SQUID, turned out to burn sometime between their room temperature resistance check and the first SQUID biasing when the system is at 4.2K.

Soon a new UHV system will be completely assembled and operated in our lab, which will allow for evaporation of superconducting thin films of niobium (Nb). Superconducting Nb films are deposited at a higher vacuum than Pb films, but do not require a cold substrate and exchange gas and have good adhesion to glasses. Moreover, Nb has a higher bulk critical temperature of 9.2K. Due to the difficulties in the Pb SQUID procedure, this is by far the promising way to proceed with this project– making Nb tips and filling them to measure the core effects.

If the results of the magnetite particles will be satisfactory, i.e. if the flux will be enhanced by a significant factor and the side effects, such as noise and magnetic saturation, will be tolerable, new nanoparticles with lower blocking temperature and perhaps a higher permeability materials should be tested. The proposed materials if they can be found in a colloidal form in liquid will be NiO[32] and also perhaps hcp-Ni[33], both showing low blocking temperatures.

Appendix A: Circuitry

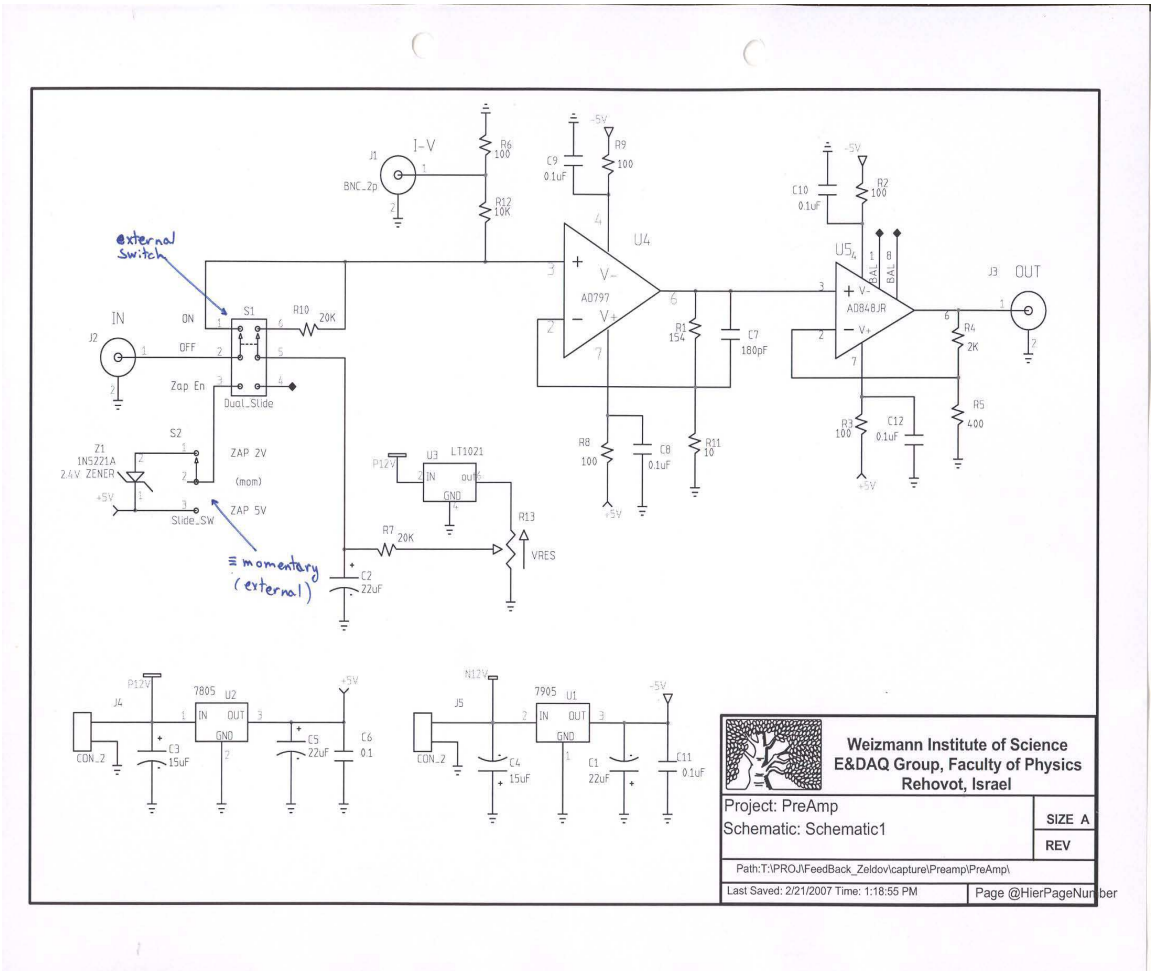

Fig. 5.1: *Pre-Amplifier box circuit.*

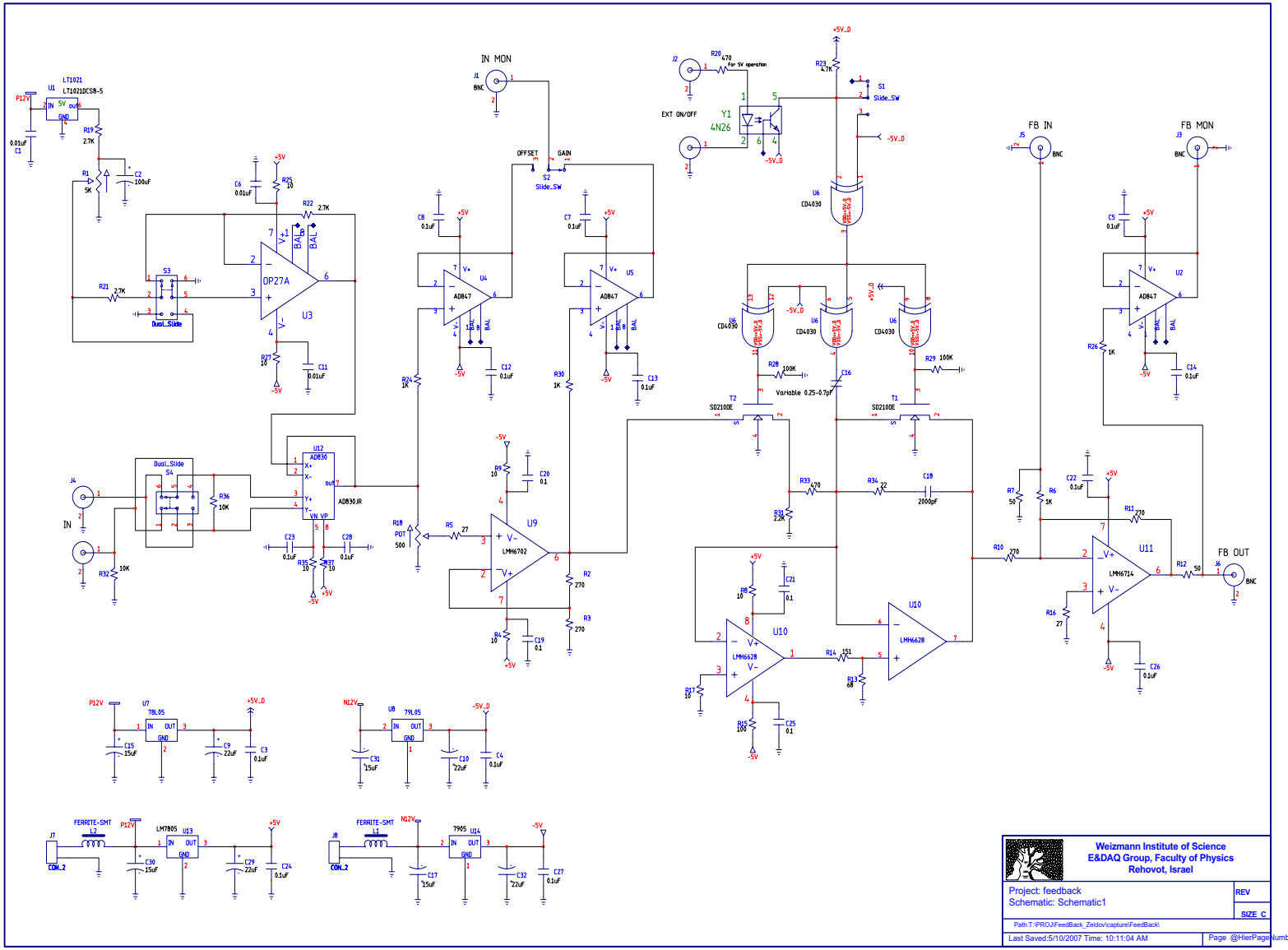

Fig. 5.2: *Feedback box circuit.*

Appendix B: Improving tuning forks production

Tuning forks (TF) are used for surface scanning in many scanning microscopes. The TF is made of quartz (piezoelectric) and has two electrodes to excite it or read from it. It has a very sharp resonance at certain frequencies (specifically 32,768 Hz for the discussed TF). When it is excited and approaching some surface, the TF "feels" it mainly by Van-Der-Waals forces and changes its frequency and amplitude. This effect is being widely used in microscopy, where the scanning tip is glued (mechanically coupled) to one of the TF's tines, see figure 5.3. The tip sticks out over the TF and detects the surface.

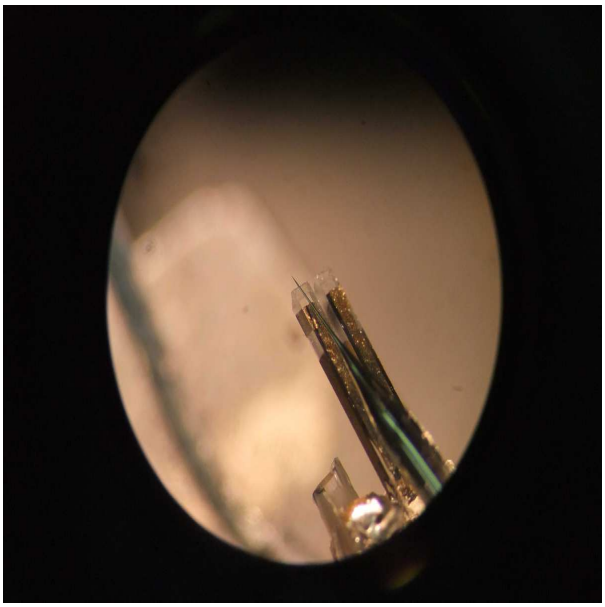

Fig. 5.3: *An image of a tip attached to a TF tine through a microscope ocular.*

The assembly of the TF setup was done manually with a poor precision and had a success rate of less than 50%. Trying to improve the precision and the success rate of the

production, a new template was designed.

The way TF's were made was (image is presented in figure 5.4 (b)):

1. The tuning fork was taken out of its vacuum can and its legs were gently removed with a soldering iron.

2. Quartz plates, that were previously plated with chromium and gold, were cut into small plate pieces. The gold were scratched to form 2 contacts and two copper wires were soldered to it. Later it was weakly glued to a microscope slide with varnish.

3. Another microscope slide was glued as a step to support the TFs and the TFs were glued to the quartz pieces with 2-part epoxy glue and then baked.

4. Silver paint was used to connect the two gold contacts to the two TF electrodes and then all was put in the oven for additional baking.

5. The 2-part epoxy was used to glue a quartz rod to the quartz plate from its back side and then baked.

6. The rod was plugged in a 15 degrees tilted socket, glued with the 2-part epoxy and baked again.

Two main problem were dominating this procedure. First is the lack of precision and repetition of the results. The tuning fork had to be mounted on a specific holder (see figure 5.4 (d)) and be glued later to a SQUID tip and if it was not glued precisely enough, there would be a mismatch between the two. The second issue came from stage 4 - the silver paint while in the oven was flowing and many times (more than 50%) shorted the TF's contacts. Such forks could not be saved and were disposed of.

The new template design came with a new holder design for the TF (see figures 5.4 (a),(c)). Step number 1 remains the same, but all the others were altered or removed:

1. The tuning fork was taken out of its vacuum can and its legs were gently removed with a soldering iron.

2. Quartz plates sized 5x5x1mm and 5x5x0.5mm were bought. 10 pieces are placed in their fitting sockets and covered with a mask that was designed (see figure 5.4 (a)) to deposit the gold contacts on designated places on the quartz.

3. The contacts are then deposited and two copper wires soldered to them.

4. The TF's are put in their designated sockets, glued with the 2-part epoxy or varnish and later baked.

5. All the contacts between the TFs and the gold pads are done with a gold wire bonder machine to avoid shorts. It is held in the bonder with vacuum that holds the pieces through holes from below.

The new template holds the pieces in place and keeps the TF position on the plates constant. The idea was to have the quartz plate pieces stay in their place from beginning to end in the template. The template is designed for two sizes of plates (around 0.5mm and 1mm) and also for dither crystals that are 5.1x5.1x0.5mm.

Another template that is being designed nowadays by lab mates is saving the need in soldering on the plates (or dithers), that can damage them, by doing all the contacts with the bonding machine.

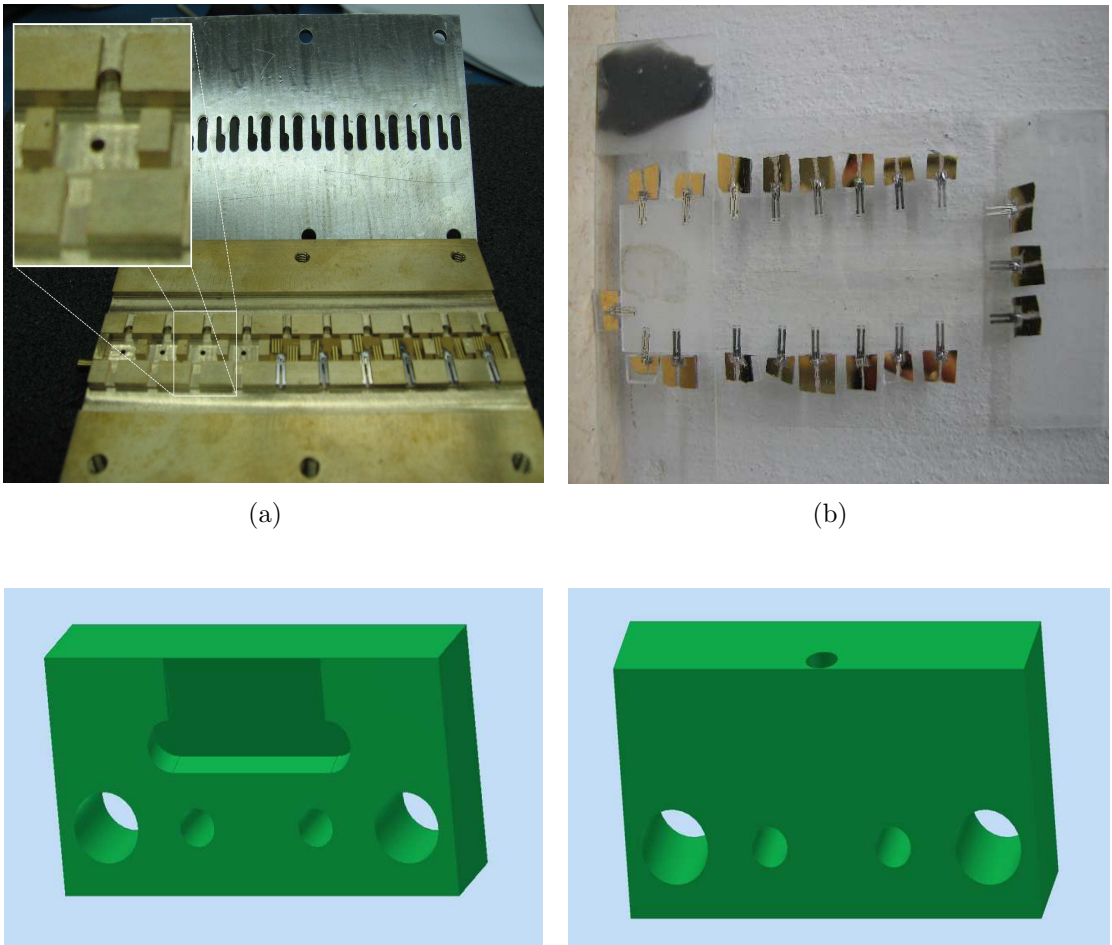

(a) (b)

(c) (d)

Fig. 5.4: *(a) The new template design made of brass (one socket is enlarged) with an aluminum mask and (b) the previous method for making tuning forks;(c) The new design for the tuning fork's holder and (d) the previous design.*

References

[1] A. Finkler, Y. Segev, Y. Myasoedov, M. L. Rappaport, L. Neeman, D. Vasyukov, E. Zeldov, M. E. Huber, J. Martin, and A. Yacoby, "Self-aligned nanoscale SQUID on a tip," *Nano Letters*, vol. 10, p. 1046, 2010.

[2] F. Bitter, "On the magnetization of ferromagnetic crystals," *Physical Review*, vol. 43, p. 655, 1933.

[3] H. F. Hess, R. B. Robinson, R. C. Dynes, J. M. Valles, and J. V. Waszczak, "Scanning-Tunneling-Microscope observation of the Abrikosov flux lattice and the density of states near and inside a fluxoid," *Phys. Rev. Lett.*, vol. 62, p. 214, 1989.

[4] A. M. Chang, H. D. Hallen, L. Harriott, H. F. Hess, H. L. Kao, J. Kwo, R. E. Miller, R. Wolfe, J. van der Ziel, and T. Y. Chang, "Scanning Hall probe microscopy," *Applied Physics Letters*, vol. 61, p. 1974, 1992.

[5] C. W. Yuan, Z. Zheng, A. L. de Lozanne, M. Tortonese, D. A. Rudman, and J. N. Eckstein, "Vortex images in thin films of $YBa_2Cu_3O_{7-x}$ and $Bi_2Sr_2Ca_1Cu_2O_{8+x}$ obtained by low-temperature magnetic force microscopy," in *Journal of Vacuum Science and Technology B*, p. 1210, 1996.

[6] J. E. Bonevich, K. Harada, T. Matsuda, H. Kasai, T. Yoshida, G. Pozzi, and A. Tonomura, "Electron holography observation of vortex lattices in a superconductor," *Phys. Rev. Lett.*, vol. 70, p. 2952, 1993.

[7] A. Mathai, D. Song, Y. Gim, and F. C. Wellstood, "One-dimensional magnetic flux microscope based on the DC superconducting quantum interference device," *Applied Physics Letters*, vol. 61, p. 598, 1992.

[8] S. A. Gudoshnikov, B. Y. Liubimov, L. V. Matveets, A. P. Mikhailenko, Y. V. Deryuzhkina, Y. S. Sitnov, and O. V. Snigirev, "Flux guide for high-T_c SQUID microscope with high spatial resolution," *Physica C: Superconductivity*, vol. 368, p. 66, 2002.

[9] S. Tanaka, K. Matsuda, O. Yamazaki, M. Natsume, H. Ota, and T. Mizoguchi, "Development of high-T_c SQUID microscope with flux guide," *Superconductor Science and Technology*, vol. 15, p. 146, 2002.

[10] T. Nagaishi, K. Minamimura, and H. Itozaki, "HTS SQUID microscope head with permalloy flux guide," *Applied Superconductivity, IEEE Transactions*, vol. 13, p. 227, 2003.

[11] B. Baek, S. H. Moon, S. Y. Lee, S. M. Lee, J. I. Kye, H. J. Lee, and Z. G. Khim, "Investigation of a magnetic flux-guide for a HTS scanning superconducting quantum interference device microscope," *Superconductor Science and Technology*, vol. 17, p. 1022, 2004.

[12] T. Hayashi, M. Tachiki, and H. Itozaki, "SQUID probe microscope combined with scanning tunneling microscope," *Applied Superconductivity, IEEE Transactions*, vol. 17, p. 792, 2007.

[13] P. Pavlov, V. Guschin, J. Y. Son, and S. H. Kim, "A magnetic flux guide for SQUID microscope," in *Multisensor Fusion and Integration for Intelligent Systems. IEEE International Conference*, pp. 147–149, 2008.

[14] H. K. Onnes, "The superconductivity of mercury," *Communications from the Physical Laboratory at Leiden University*, 1911.

[15] J. Bardeen, L. N. Cooper, and J. R. Schrieffer, "Theory of superconductivity," *Physical Review*, vol. 108, p. 1175, 1957.

[16] J. G. Bednorz and K. A. Müller, "Possible high T_c superconductivity in the Ba-La-Cu-O system," *Zeitschrift für Physik B Condensed Matter*, vol. 64, p. 189, 1986.

[17] V. L. Ginzburg and L. D. Landau, "On the theory of superconductivity," *Zhurnal Eksperimentalnoi I Teoreticheskoi Fisiki*, vol. 20, p. 1064, 1950.

[18] L. P. Gor'kov, "Microscopic derivation of the Ginzburg-Landau equations in the theory of superconductivity," *Soviet Physics JETP*, vol. 9, p. 1364, 1959.

[19] A. A. Abrikosov, "On the magnetic properties of superconductors of the second group," *Soviet Physics JETP*, vol. 5, p. 1174, 1957.

[20] B. D. Josephson, "Possible new effects in superconductive tunnelling," *Physics Letters*, vol. 1, p. 251, 1962.

[21] M. Tinkham, *Introduction to Superconductivity.* Dover Publications, Inc., 2 ed., 1996.

[22] D. R. Lide, ed., *CRC Handbook of Chemistry and Physics.* Taylor and Francis, 86th ed., Internet version 2006.

[23] D. S. Golubovic and V. V. Moshchalkov, "Linear magnetic flux amplifier," *Applied Physics Letters*, vol. 87, p. 142501, 2005.

[24] J. Frenkel and J. Dorfman, "Spontanous and induced magnetisaion in ferromagnetic bodies," *Nature*, vol. 126, p. 274, 1930.

[25] G. Schmid, ed., *Nanoparticles - from theory to application.* Wiley-VCH, 2004.

[26] L. Neel, "Thermoremanent magnetization of fine powders," *Reviews of Modern Physics*, vol. 25, p. 293, 1953.

[27] I. S. Jacobs and C. P. Bean, *Magnetism*, vol. III - Spin Arrangement and Crystal Structure, Domains, and Micromagnetics. Academic Press - New York and London, 1963.

[28] J. Lin, W. Zhou, A. Kumbhar, J. Wiemann, J. Fang, E. E. Carpenter, and C. J. O'Connor, "Gold-coated iron (Fe@Au) nanoparticles: Synthesis, characterization, and magnetic field-induced self-assembly," *Journal of Solid State Chemistry*, vol. 159, p. 26, 2001.

[29] C. T. Seip, E. E. Carpenter, C. O'Connor, V. T. John, and S. Li, "Magnetic properties of a series of ferrite nanoparticles synthesized in reverse micelles," *Magnetics, IEEE Transactions*, vol. 34, p. 1111, 1998.

[30] G. F. Goya, T. S. Berquo, F. C. Fonseca, and M. P. Morales, "Static and dynamic magnetic properties of spherical magnetite nanoparticles," *Journal of Applied Physics*, vol. 94, p. 3520, 2003.

[31] I. W. Park, M. Yoon, Y. M. Kim, Y. Kim, H. Yoon, H. J. Song, V. Volkov, A. Avilov, and Y. J. Park, "Magnetic properties and microstructure of cobalt nanoparticles in a polymer film," *Solid State Communications*, vol. 126, p. 385, 2003.

[32] J. Park, E. Kang, S. U. Son, H. M. Park, M. K. Lee, J. Kim, K. W. Kim, H. J. Noh, J. H. Park, C. J. Bae, J. G. Park, and T. Hyeon, "Monodisperse nanoparticles of Ni and NiO: Synthesis, characterization, self-assembled superlattices, and catalytic applications in the Suzuki coupling reaction," *Advanced Materials*, vol. 17, p. 429, 2005.

[33] Y. Chen, D. L. Peng, D. Lin, and X. Luo, "Preparation and magnetic properties of nickel nanoparticles via the thermal decomposition of nickel organometallic precursor in alkylamines," *Nanotechnology*, vol. 18, p. 505703, 2007.

[34] M. Huber, P. Neil, R. Benson, D. Burns, A. Corey, C. Flynn, Y. Kitaygorodskaya, O. Massihzadeh, J. Martinis, and G. Hilton, "DC SQUID series array amplifiers with 120 MHz bandwidth (corrected)," *Applied Superconductivity, IEEE Transactions*, vol. 11, p. 4048, 2001.

[35] C. M. Cotell, J. A. Sprague, and F. A. J. Smidt, eds., *ASM Metals Handbook Vol. 5 - Surface Engineering*. ASM International, 1994.

[36] T. A. Fulton, L. N. Dunkleberger, and R. C. Dynes, "Quantum interference properties of double Josephson junctions," *Physical Review B*, vol. 6, p. 855, 1972.

[37] M. Cyrot, "Ginzburg-Landau theory for superconductors," *Reports on Progress in Physics*, vol. 36, p. 103, 1973.

[38] J. Clarke and A. I. Braginski, eds., *The SQUID Handbook: Fundamentals and Technology of SQUIDs and SQUID Systems*, vol. I. Berlin: Wiley, 2004.